Progress in Oceanography 202 (2022) 102756

Contents lists available at ScienceDirect

Progress in Oceanography

journal homepage: www.elsevier.com/locate/pocean

Nutrient streams in the North Pacific

Yu Long [a,b], Xinyu Guo [a,c,*], Xiao-Hua Zhu [a,b,d], Zhiyuan Li [e]

[a] State Key Laboratory of Satellite Ocean Environment Dynamics, Second Institute of Oceanography, Ministry of Natural Resources, Hangzhou 310012, China
[b] Southern Marine Science and Engineering Guangdong Laboratory (Zhuhai), Zhuhai, 519082, China
[c] Center for Marine Environmental Study, Ehime University, 2-5 Bunkyo-cho, Matsuyama 790-8577, Japan
[d] School of Oceanography, Shanghai Jiao Tong University, Shanghai, 200030, China
[e] Key Laboratory for Technology in Rural Water Management of Zhejiang, Zhejiang University of Water Resources and Electric Power, Hangzhou 310018, China

ARTICLE INFO

Keywords:
Nutrient stream
North Pacific
Nutrient transport
World Ocean Circulation Experiment
Inverse method

ABSTRACT

The nutrient streams in the North Pacific were examined by analyzing the results derived from the inverse calculation of the World Ocean Circulation Experiment (WOCE)-revisit cruise data. The Kuroshio, Alaskan Stream, and Oyashio drive the most intensive nutrient transport within the basin. The upper portion of the nutrient stream (lighter than 26.2 kg/m^3) contains mode waters and recirculates within the subtropical gyre, while the intermediate portion (26.2–27.15 kg/m^3) relates to North Pacific Intermediate Water (NPIW) and contributes most to nutrient transport in the nutrient stream. The nutrient concentration in the nutrient stream increases in the subtropical gyre along the Kuroshio and Kuroshio Extensions but decreases in the subarctic gyre from the Alaskan Stream to the Oyashio region. This increase or decrease in nutrient concentration from the upstream region to the downstream region mainly results from lateral water exchange, although it also partly depends on biogeochemical processes and vertical diffusion. Specifically, the lateral exchange of the nutrient stream in the subarctic gyre with water from lower latitudes decreases the nitrate concentration of the Alaskan Stream and that with water from the Okhotsk Sea decreases the nitrate concentration of the Oyashio. For vertical nitrate transport, our estimation shows that the ventilation processes of subduction and induction are comparable to the sum of vertical advection and diffusion. This implies that nutrient transport related to the ventilation of the North Pacific is in a dynamic balance on an annual cycle and should be quantified in future work.

1. Introduction

The ocean circulation in the North Pacific features two gyres, which are the clockwise subtropical gyre that includes the Kuroshio and its extension, the North Pacific Current, the California Current and the North Equatorial Current, and the anticlockwise subarctic gyre, which includes the Alaskan gyre and the Western Subarctic Gyre. The two gyres encounter the Kuroshio Extension region, where warm, saline, and nutrient-depleted subtropical waters are mixed with cold, fresh, and nutrient-rich subarctic water and where mode water, for example, Subtropical Mode Water and Central Mode Water, and North Pacific Intermediate Water (NPIW) form. Ocean currents transport (export) nutrients within (between) gyres, supporting local and basin-scale primary productivity.

The importance of large-scale nutrient transport has been addressed in many studies. Pelegri and Csanady (1991) and Pelegrí et al. (1996) examined nutrient transport by the Gulf Stream and proposed that the Gulf Stream provides nutrients to the subpolar North Atlantic Ocean and that both vertical and lateral processes are important to the supply of nutrients along the stream. Sarmiento et al. (2004) revealed the significant role of high-latitude nutrient export in supporting primary productivity in low-latitude regions and suggested that NPIW formation was responsible for 70% of the silicic acid supply to diatom production. Letscher et al. (2016) demonstrated that lateral transport accounts for 24–36% of the nitrogen and 44–67% of the phosphorus supply in gyre margins. Their study confirmed again that lateral processes were as important as vertical processes to local primary production and they agreed with the conclusion given by Lozier et al. (2011) that the interannual variability in oceanic productivity depends not only on wind and buoyancy forcing but also on subsurface advective nutrient supply to the surface rather than on local stratification.

Generally, the western boundary currents have the most intensive

* Corresponding author at: State Key Laboratory of Satellite Ocean Environment Dynamics, Second Institute of Oceanography, Ministry of Natural Resources, Hangzhou 310012, China.
E-mail address: guoxinyu@sci.ehime-u.ac.jp (X. Guo).

https://doi.org/10.1016/j.pocean.2022.102756
Received 7 July 2021; Received in revised form 24 January 2022; Accepted 8 February 2022
Available online 16 February 2022

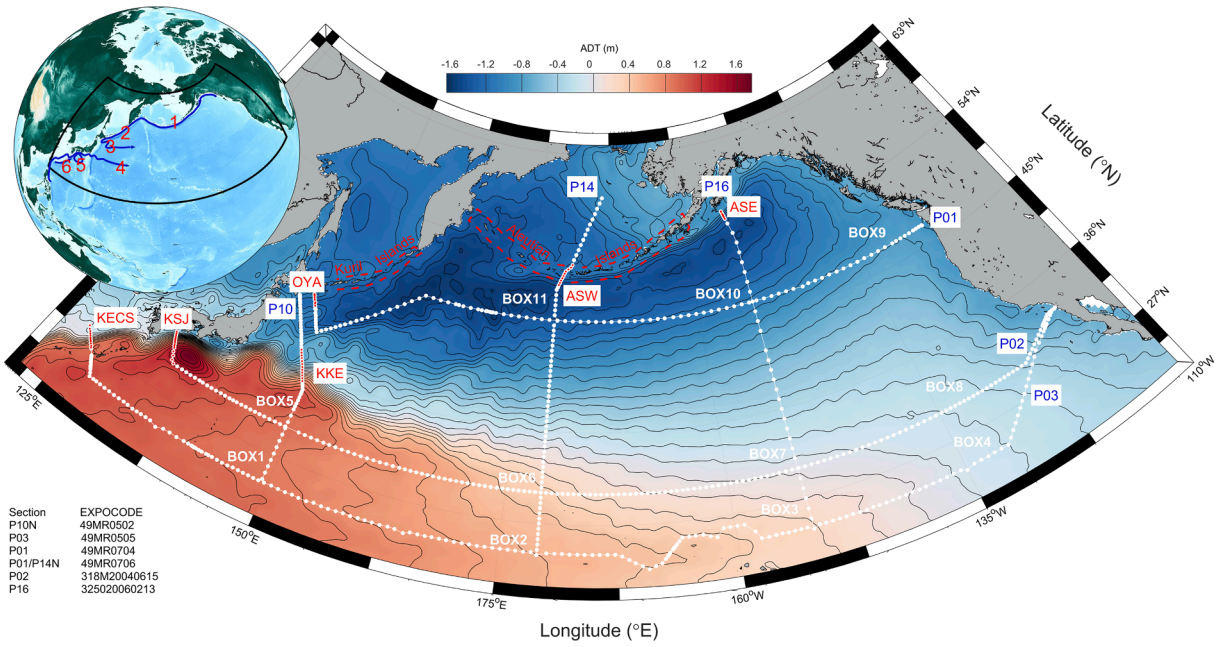

Fig. 1. Location of hydrographic data (white dots) and mean sea level (color shading) of the North Pacific. Red characters in the globe denote the main currents: 1. Alaskan Stream, 2. East Kamchatka Current, 3. Oyashio, 4. Kuroshio, 5. Kuroshio recirculation, and 6. Ryukyu Current. Red dots overlapping the white dots denote the subsections used to represent the nutrient stream. Red characters represent the name of subsections. Blue characters at the endpoint of the sections represent their names and correspond to their ExpoCode at the lower left. White characters denote the number of the box.

nutrient transport. The downward decreased velocity of the boundary currents, together with increased nutrient concentration, result in the subsurface maximum nutrient flux. As suggested by Pelegri and Csanady (1991), the Gulf Stream forms a nutrient stream acting as a giant conduit underneath the sea surface, transporting nutrients from low-latitude to high-latitude regions. The nutrient sources of the Gulf Stream are the Mode Waters from the Southern Ocean and the tropics (Williams et al., 2006; Palter and Lozier 2008). Both area-weighted (section-averaged nutrient concentration with each data point having a weight defined by the product of the distance between two hydrographic stations and the layer thickness represented by the data) and transport-weighted (nutrient transport divided by the volume transport through the same section) nutrient concentrations increase along the nutrient stream, which is caused mainly by lateral water exchange rather than by diapycnal mixing (Palter and Lozier, 2008; Williams et al., 2011). Forty percent of the transport of the Gulf Stream nutrient stream is inducted into the mixed layer in the downstream area, which supplies nutrients to isopycnals cropping out in the subpolar gyre, while the rest recirculates locally (Williams et al., 2006). Recently, Pelegrí et al. (2019) reviewed the progress of the Gulf Stream nutrient stream in the Atlantic, from the nutrient-bearing stratum (Csanady, 1990) to the role of the nutrient stream in the Earth system.

In the North Pacific, Chen et al. (1994) first revealed the multicore structure in the subsurface maximum of Kuroshio nutrient flux east of Taiwan. Guo et al. (2012, 2013) and Long et al. (2018) examined the mean state and long-term variations in the Kuroshio nutrient stream from the East China Sea (ECS) to the area south of Japan. Their findings indicated that the subsurface nutrient flux maximum of the Kuroshio is at a depth of 400 m; the Kuroshio nutrient stream south of Japan represents the confluence of the ECS Kuroshio (~170 kmolN/s), the Ryukyu current (~350 kmolN/s), and the Kuroshio recirculation south of Japan (~700 kmolN/s); and the variation in nutrient concentration along the Kuroshio is mainly due to lateral water exchange, especially in the deep layers. Additionally, Long et al. (2019) reported that the equatorward nitrate transport of the Oyashio reaches approximately 350 kmolN/s, and it exports 24 kmolN/s to the subtropical gyre along with the formation of NPIW. Nishioka et al. (2013) demonstrated that intensive mixing along the Kuril Island chain is responsible for iron export from the Okhotsk Sea to NPIW. Although the significance of the nutrient stream has been addressed, the spatial pattern of nutrient transport in the North Pacific remains unclear.

On a basin scale, Ganachaud and Wunsch (2002) used the inverse box model to calculate the velocity across transoceanic sections and estimated the transport of silicate, nitrate, phosphorus, and oxygen. They found that meridional nitrate transport is approximately 10 kmolN/s southward in the North Pacific (Section P3 in their Fig. 3, approximately 24°N) and approximately 270 kmolN/s northward in the South Pacific (Section P21 in their Fig. 3, approximately 17°S). The nutrient transport of the Indonesian throughflow (ITF) is approximately 260 kmolN/s (Ayers et al., 2014). The nutrient budget within the enclosed area bounded by Sections P3 and P21 and the ITF is almost balanced. These results may lead to the conclusion that direct transport of nutrients occurs from the South Pacific to the ITF. However, Gordon et al. (1994) suggested that a sizable proportion of ITF originates in the North Pacific. Therefore, the plausible explanation is that the northward nutrient transport almost equals the southward transport at Section P3 and that both could be large and may have different origins. If so, information about the spatial patterns of nutrient transport, as well as the nutrient streams in the North Pacific, is crucial to determine the nutrient export of the North Pacific at 24°N.

Advection also plays an important role in the nutrient supply between the thermocline and mixed layer through the ventilation process, i.e., subduction and induction. By definition (Qiu and Huang, 1995), subduction occurs mainly in the subtropical gyre, where the seawater in the mixed layer enters the permanent thermocline, and induction occurs in the subpolar gyres, where the seawater flows from the permanent thermocline to the mixed layer. Pelegrí et al. (1996, 2006) and Williams et al. (2006) demonstrated the nutrient transport of the Gulf Stream and that their induction into the mixed layer plays an important role in maintaining primary production in the North Atlantic Ocean. On the other hand, the mode water formation connects closely to subduction (Suga et al., 2008), which depends closely on the dynamic status of the Kuroshio and Kuroshio Extension (Qiu and Chen, 2006). Palter et al. (2005) suggested that the formation of mode water in the North Atlantic

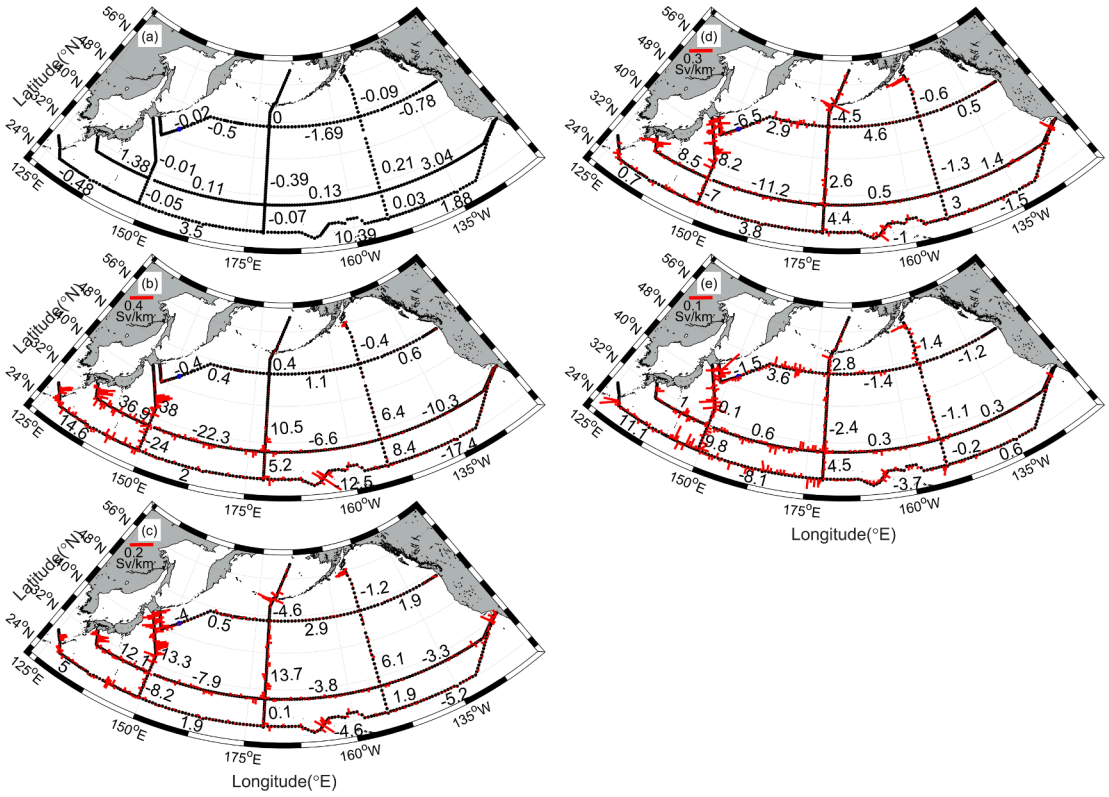

Fig. 2. Spatial pattern of volume transport. (a) Ekman component, (b) sea surface-26.2 kg/m^3, (c) 26.2–27.15 kg/m^3, (d) 27.15–27.6 kg/m^3, and (e) 27.6–27.9 kg/m^3. Numbers denote the volume transport of the adjacent section (Sv). Positive values denote northward or eastward directions. Red bars represent the volume transport per unit width (Sv/km, the volume transport over a station pair divided by the distance between the station pair). Western part of P2 and P3 represents the Kuroshio and that of P1 represents the Oyashio. The northern part of Sections P14 and P16 represents the Alaskan Stream.

subtropical region might induce spatial and temporal variability in the subsurface nutrient reservoir and may affect primary productivity in its downstream region.

Nishioka et al. (2020) recently suggested that the subpolar marginal seas supply nutrients to the North Pacific through the formation and advection of intermediate water and proposed the concept of the subarctic intermediate nutrient pool. It includes the intermediate layers of the subarctic North Pacific and its marginal seas. Although the Okhotsk Sea exports iron to the North Pacific, its role in the transport of macronutrients, such as nitrate, remains unclear. Here, the role of the Bering Sea in nutrient concentration variation along the subarctic gyre was also investigated as another candidate of the subarctic intermediate nutrient pool. As a natural hypothesis, the water exchange between these marginal seas and the North Pacific should change the nutrient concentration along the nutrient stream.

In addition to nutrient transport, the variation in nutrient concentrations along the nutrient streams is also a compelling aspect. Williams et al. (2011) suggested that diapycnal mixing, biological consumption and regeneration, and lateral water exchange are the main mechanisms responsible for this variation. Diapycnal mixing provides an upward nutrient flux from nutrient-rich deep water to nutrient-depleted surface water and can cause an increase in surface nutrient concentration along the stream path. Biological consumption and regeneration are the sink and source terms for the surface layer and deep layer, respectively, and can cause a decrease in nutrient concentration along the stream path in the surface layer and an increase in nutrient concentration along the stream path in the deep layer. Lateral water exchange results in both positive and negative variations in the nutrient concentration along the stream path, depending on the nutrient concentration in the adjacent water involved in this process.

This study is structured as follows: the data and methods are briefly described in the next section, and the spatial patterns of volume transport and nutrient transport within several isopycnal layers are shown in Section 3. The subtropical nutrient stream and subarctic nutrient stream are presented in Sections 4 and 5, respectively. The vertical nutrient transport due to vertical advection, vertical diffusion, and ventilation processes are examined in Section 6, and concluding remarks are provided in Section 7.

2. Data and methods

The hydrographic data used in this study geographically encompassed most of the North Pacific and were observed by World Ocean Circulation Experiment (WOCE)-revisit cruises during 2004–2007 (Fig. 1). The conductivity–temperature–depth (CTD) data for the full depth, with a vertical resolution of 1 or 2 dbar, together with nitrate, silicate, and phosphate concentrations of up to 36 levels, were used in the box model analysis. The data are available on the CCHDO (CLIVAR and Carbon Hydrographic Data Office) website. Hydrographic data from the Japan Meteorological Agency (JMA) and Japan Agency for Marine-Earth Science and Technology (JAMSTEC) were also used to show the nitrate concentrations in the Okhotsk Sea and Bering Sea, respectively.

The absolute geostrophic velocity at each section was calculated using the inverse method (Wunsch, 1978) (details are presented in the Appendix). After the absolute geostrophic velocity was determined, the nitrate flux was calculated by multiplying it by the nitrate concentration, and nitrate transport was obtained by integrating the nitrate flux over the section. The focus of this study was the nutrient stream, which is mainly determined by the upper layer circulation, and therefore, this analysis was limited to the results in the upper 2000 m. Nitrate flux was chosen to represent the nutrient streams. Phosphate flux and silicate flux have a similar spatial distribution to nitrate flux, and their transport can be approximately obtained by the Redfield ratio and nitrate transport.

Because the cruises were carried out in different months, the data

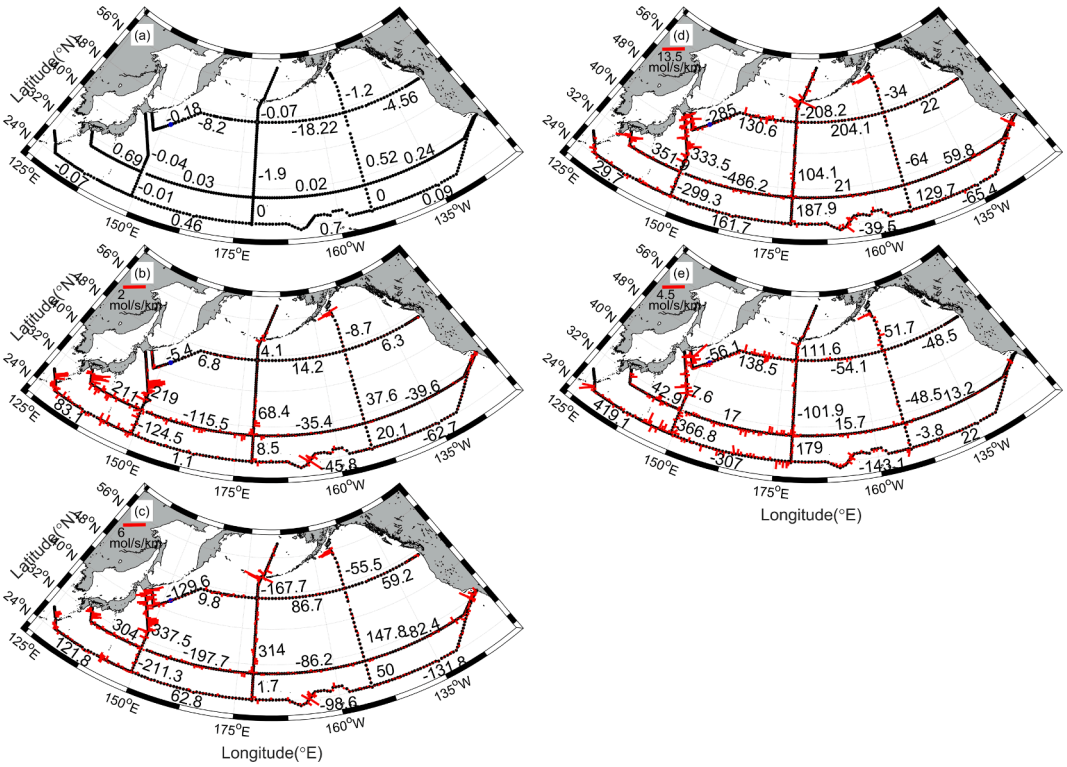

Fig. 3. Spatial pattern of nitrate transport. (a) Ekman component, (b) sea surface-26.2 kg/m^3, (c) 26.2–27.15 kg/m^3, (d) 27.15–27.6 kg/m^3, and (e) 27.6–27.9 kg/m^3. Numbers denote the nutrient transport of the adjacent section (kmol/s). Positive values denote northward or eastward directions. Red bars represent the nutrient transport per unit width (mol/s/km, the nitrate transport through a station pair divided by the distance between a station pair). Western part of P2 and P3 represents the Kuroshio and that of P1 represents the Oyashio. The northern part of Sections P14 and P16 represents the Alaskan Stream.

include not only spatial variation but also temporal variations, especially in the upper layer (first and second layers in our inverse model). Due to this factor, our analysis of the nitrate concentration along the stream was limited to the layers from the third layer. The regeneration process, which converts organic nitrogen to nitrate, was analyzed. The regenerated nitrate concentration (C_{reg}) was estimated from the apparent oxygen utilization (AOU, the difference between the saturation oxygen concentration calculated from in situ temperature and salinity and the observed dissolved oxygen concentration from the same sample) by assuming $C_{reg} = -AOU/R$, where the Redfield ratio R was taken as O_2:N = −170:16 (Sarmiento and Gruber, 2006). The regeneration rate is the ratio of regenerated nitrate concentration to the measured nitrate concentration and is related to the duration since the latest ventilation of the observed water mass.

3. Spatial pattern of nutrient transport

The large-scale flow pattern derived from the inverse method is generally consistent with the understanding of the upper layer circulation in the North Pacific. The box model encompassed the northern half of the subtropical gyre and the entire subarctic gyre. The boundary currents, that is, the Kuroshio, Oyashio, and Alaskan Stream, can be recognized by the large volume transport per unit width at the boundaries of the basin (Fig. 2).

According to the typical distribution of the water mass, the volume transports within four isopycnal layers were presented. These included the surface layer where the central water and mode water exist (sea surface–26.2 kg/m^3 with a typical thickness of 400 m in the subtropical gyre and 50–100 m in the subarctic gyre (Fig. 2b)), the intermediate layer where the NPIW exists (26.2–27.15 kg/m^3 with a typical thickness of 350–400 m (Fig. 2c)), the deep layer (27.15–27.6 kg/m^3 from the bottom of NPIW to a depth of approximately 1000 m (Fig. 2d)), and the bottom layer (27.6–27.9 kg/m^3 from a depth of approximately 1000 m to 2000 m (Fig. 2e)).

The Ekman components of volume transport at Sections P1, P2, and P3 generally decrease from south to north (Fig. 2a), while nitrate transport increases from south to north (Fig. 3a) because of the northward increase in the surface nitrate concentration. Transport in the surface layer appears mostly in the subtropical gyre (Fig. 2b). For the section corresponding to the Kuroshio (western-most part of P2), the transport in the surface layer explains 63% of the total volume transport (Fig. 2b, the volume transport of the surface layer divides that of the upper 2000 m, that is, 36.9 Sv/(36.9 + 12.1 + 8.5 + 1) Sv)), and 23% of the nitrate transport (Fig. 3b, the nitrate transport of the surface layer divides that of the upper 2000 m, 211.7 kmolN/s/(211.7 + 304 + 351.9 + 42.9) kmolN/s) in the upper 2000 m. The lower ratio of the nitrate transport is because the nitrate concentration is lower in this layer than in the other layers.

The intermediate layer where the NPIW exists is ventilated directly in the subarctic gyre but indirectly in the subtropical gyre through NPIW formation (Talley et al., 1995). The values in this layer explain approximately 21% (32%) of the volume transport (Fig. 2c) and 33% (27%) of the nitrate transport (Fig. 3c) in the upper 2000 m (numbers prior to the parentheses represent the Kuroshio in the western part of Section P2; the numbers in the parentheses represent the Oyashio in the western part of Section P1). When considering the layer thickness, its nitrate transport is the most intensive among all layers (Fig. 3). The flow pattern shows that the western portion of Section P01 (Fig. 2c), i.e., the Oyashio, is the only advective pathway for subarctic water exported to the subtropical gyre. It has an approximately 4 Sv volume transport, which is consistent with that given by Talley et al. (1995). Nitrate transport is approximately 130 kmolN/s (Fig. 3c), which agrees with the value estimated from different datasets (Long et al., 2019). Apart from the Oyashio, the volume transport in the eastern part of Section P1 is northward, indicating a poleward transport of the lower nutrient concentration seawater from the subtropical gyre.

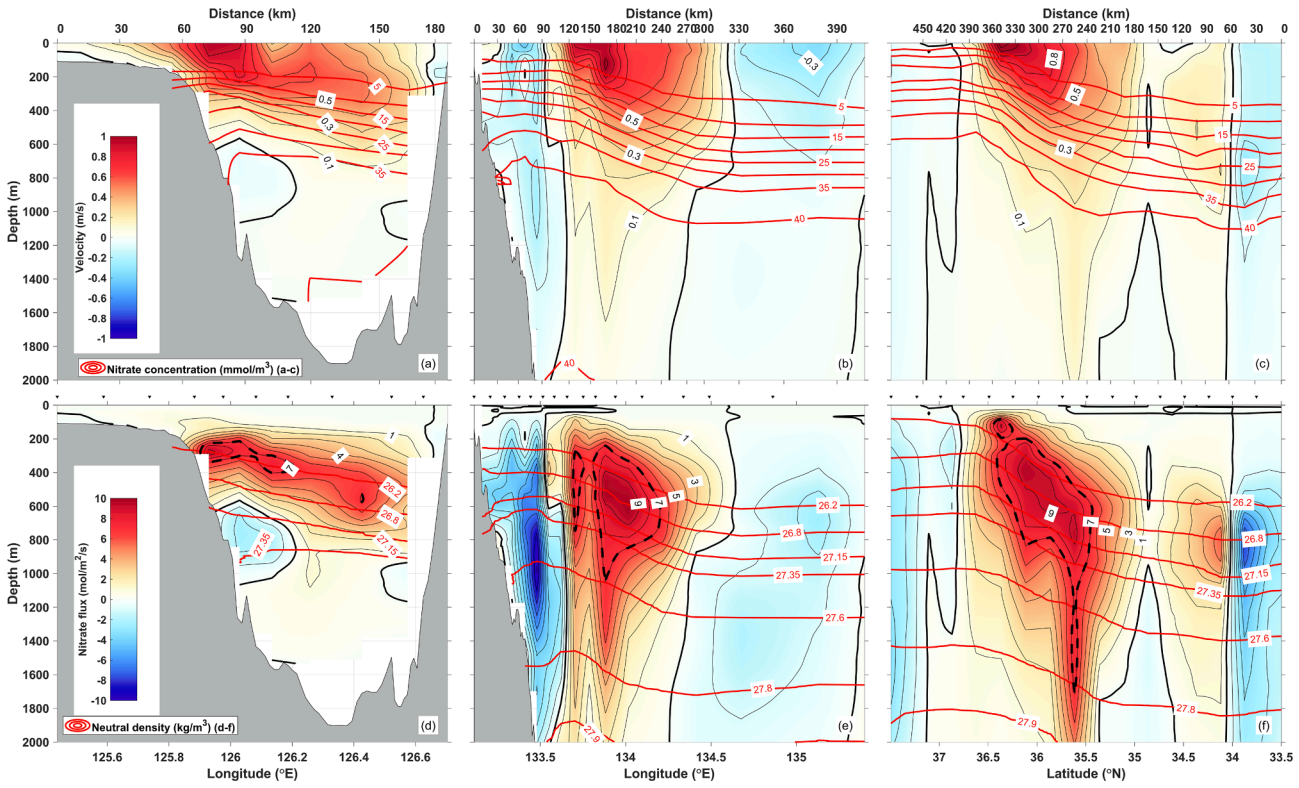

Fig. 4. Velocity and nitrate flux along the Kuroshio. (a), (b), and (c) show the velocity of the Kuroshio in the ECS (at Section P03), south of Japan (at Section P02), and the Kuroshio Extension (at Section P10). Red contours denote the nitrate concentration (mmol/m^3). (d), (e), and (f) represent the nitrate flux for the KECS, KSJ, and KKE, respectively. Red contours denote the neutral density surface (kg/m^3). The black dashed line denotes a contour of 7 mmol/m^2/s for nitrate flux. Positive and negative values indicate eastward and westward directions, respectively.

Table 1
Volume transport (Vt), nitrate transport (Nt), transport weighted nitrate concentration (Ct) and area weighted nitrate concentration (Ca) within seven isopycnal layers for the section in the ECS (at section P03), south of Japan (at section P02), and the Kuroshio Extension (at section P10). The numbers in the first column are the index of isopycnal layers, 'T' means total water column, and red and blue characters denote increasing and decreasing of nitrate concentration along the stream path. The lower boundary of the layers is 26.2, 26.8, 27.15, 27.35, 27.6, 27.8, and 27.9 kg/m^3. Positive (negative) values indicate northward (southward) or eastward (westward).

	Vt (Sv)			Nt (kmol/s)			Ct (mmol/m^3)			Ca (mmol/m^3)		
	KECS	KSJ	KKE	KECS	KSJ	KKE	KECS	KSJ	KKE	KECS	KSJ	KKE
T	**30**	**78.19**	**81.13**	**315.88**	**1215.95**	**1578.06**	N/A	N/A	N/A	N/A	N/A	N/A
1	23.00	49.14	42.24	125.90	262.26	246.94	5.47	5.34	5.85	5.33	5.94	5.67
2	4.22	8.97	11.11	100.14	205.13	246.98	23.72	22.86	22.24	23.75	22.82	22.13
3	1.41	5.54	7.71	45.62	182.11	259.49	32.46	32.90	33.66	31.89	32.35	32.84
4	0.37	2.79	4.59	14.02	108.55	184.44	37.72	38.89	40.17	35.90	37.71	39.21
5	1.00	5.02	6.31	39.29	208.88	274.03	39.31	41.59	43.41	39.03	40.29	42.39
6	N/A	4.71	5.93	N/A	201.16	268.73	N/A	42.68	45.34	N/A	41.24	43.90
7	N/A	2.02	3.24	N/A	84.75	146.00	N/A	42.05	45.05	N/A	40.54	43.43

The deep layer (Figs. 2d and 3d) and the bottom layer (Figs. 2e and 3e) show reductions in volume transport and nitrate transport. These layers are deep portions of the nutrient stream, accounting for one-seventh of the volume transport and more than half of the nitrate transport within the entire water column, which results from the high nutrient concentration of the deep water. These layers export nutrients to the intermediate layer through vertical advection and vertical diffusion and are too deep to directly influence local primary productivity.

The nutrient stream is defined by the large values of volume transport and nitrate transport per unit width in the boundary current region, particularly in the intermediate layer (Fig. 3). Following this definition, sections across the Kuroshio in the subtropical gyre and those across the Oyashio and Alaskan Streams in the subarctic gyre were chosen to represent the nutrient streams in the North Pacific.

4. Subtropical nutrient streams

The subtropical nutrient stream is associated with the Kuroshio. The width of the Kuroshio increases in the downstream direction (Fig. 4a–c) from the ECS (KECS, Section P03, Fig. 1) to the area south of Japan (KSJ, Section P02) and further to the Kuroshio Extension (KKE, Section P10). This is mainly attributed to the presence of the Kuroshio recirculation gyre (negative values in Fig. 4b, c) that joins the Kuroshio and becomes a part of the eastward current in the Kuroshio. Consequently, the eastward volume transport varies from 30.0 (KECS) to 78.2 (KSJ) to 81.1 Sv (KKE) (Table 1). The vertical structure of nitrate concentration changes little among the three sections, and the nutricline, for example, the contour of 15 mmolN/m^3, is located at a depth of approximately 300–800 m (Fig. 4a–c).

The nitrate flux is intensified from the KECS to KKE (Fig. 4d–f). For

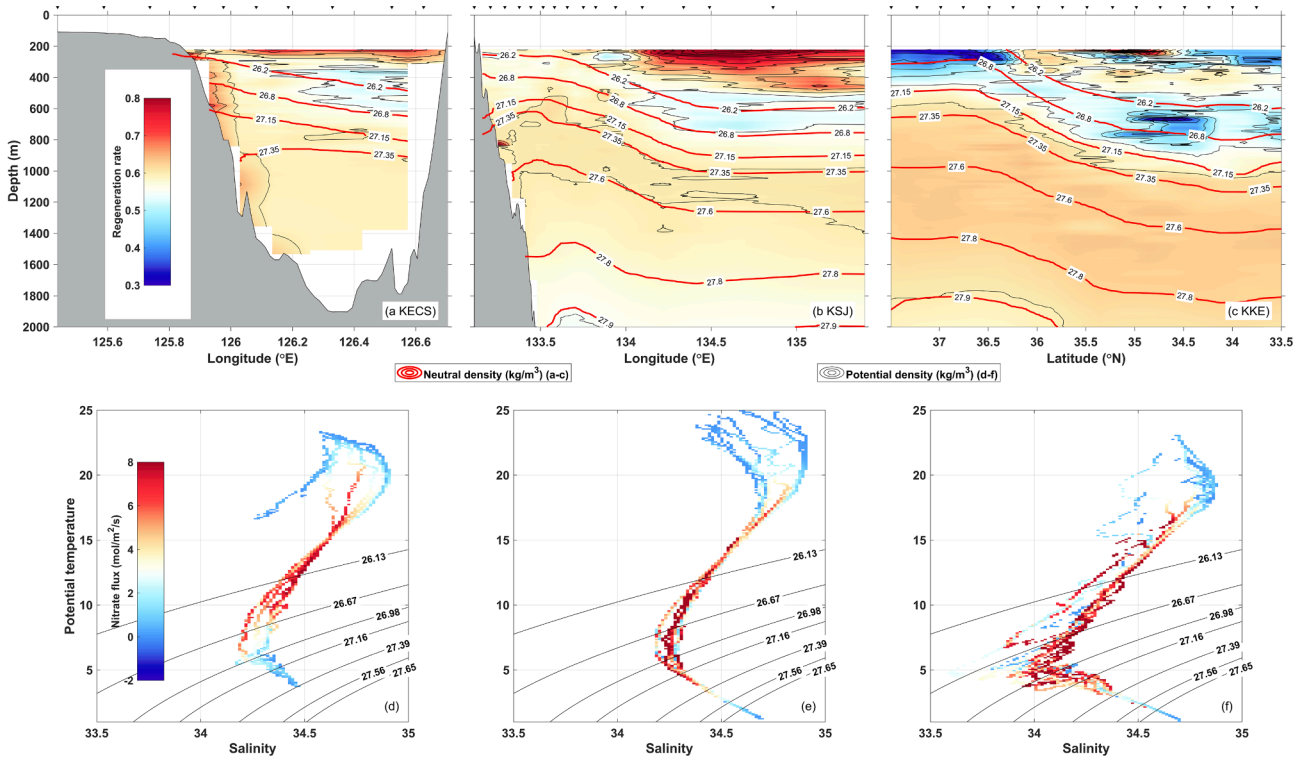

Fig. 5. (a), (b), and (c) represent the ratio of regenerated nitrate concentration to nitrate concentration of the Kuroshio in the ECS (at Section P03), south of Japan (at Section P02), and the Kuroshio Extension (at Section P10). Red contours denote the neutral density surface (kg/m^3). The top layer is blank due to the large uncertainties. (d), (e), and (f) represent the temperature-salinity diagram, and color shading denotes the nitrate flux for the KECS, KSJ, and KKE, respectively. Potential density contours 26.13, 26.67, 26.98, 27.16, 27.39, 27.56, and 27.65 in (d–f) correspond to neutral densities of 26.2, 26.8, 27.15, 27.35, 27.6, 27.8, and 27.9, respectively.

example, the subsurface maximum core (defined by the contour of 7 mmolN/m^2/s in Fig. 4d–f) varies in size, depth (350–600 m for the KECS, 400–700 m for the KSJ, and 300–800 m for the KKE), and density range (26.2–26.8 kg/m^3 for the KECS, 26.2–27.15 kg/m^3 for the KSJ, and 26.2–27.15 kg/m^3 for the KKE). The nitrate flux subsurface cores of the KECS, KSJ, and KKE are generally located within the NPIW range (26.2–27.15 kg/m^3), implying that the nutrient stream is closely related to NPIW. In addition, nitrate transport varies from 315.9 (KECS) to 1216.0 (KSJ) to 1578.0 (KKE) kmolN/s. The nitrate transport of the KECS and KSJ is close to the values reported by Guo et al. (2013), while that of the KKE is the first to be reported.

Notably, from the KSJ to KKE, the volume transport increases by approximately 3 Sv, while the nitrate transport increases by approximately 360 kmolN/s. The volume transport difference between the KSJ and KKE in each layer (Table 1) shows that there is a decrease of approximately 7 Sv in the surface layer and an increase of approximately 10 Sv within layers 2–7. Consequently, nitrate transport decreases by 15 kmolN/s in the surface layer but increases by 389 kmolN/s in layers 2–7. Therefore, the large nitrate transport increase from the KSJ to KKE results from the lateral water exchange that exports nutrient-poor water in the surface layer but imports nutrient-rich water in the subsurface and deep layers.

Both the area-weighted and transport-weighted nitrate concentrations increase along the Kuroshio in deep layers 3–7 (Table 1). The nitrate concentration variation along the Kuroshio from the KECS to KSJ was examined and was concluded to be caused primarily by lateral water exchange (Guo et al., 2013; Long et al., 2018); therefore, the main focus here was on the KKE section. Following Williams et al. (2011), the role of regeneration, diapycnal mixing, and lateral water exchange in changing the nitrate concentration along the Kuroshio nutrient stream was examined.

Fig. 5 shows the regeneration rate of nitrate (Fig. 5a–c) and the T-S relationship (Fig. 5d–f). For the Kuroshio from the KECS to KSJ, the regeneration rate of nitrate (Fig. 5a, b) and the T-S relationship (Fig. 5d, e) change little. For the Kuroshio from the KSJ to KKE, the regeneration rate (Fig. 5b, c) decreases in the intermediate layer but slightly increases in the deep layer. Combined with the increased nitrate concentration from the KSJ to KKE, it is suggested that the water mass involved in lateral water exchange has a low regeneration rate and a high nitrate concentration. Since the newly ventilated water has a low regeneration rate but a high nitrate concentration, the decreases in regeneration rate from the KSJ to KKE should be caused by lateral water exchange with newly ventilated water. The zigzag T-S relationship (Fig. 5f) in the intermediate layer in the KKE confirms the intense water mixing in the salinity minimum layer and its close relationship with NPIW formation (Talley et al., 1995); that is, the Kuroshio and Oyashio mix in the mixed water region and export the newly ventilated water from the subarctic gyre to the subtropical gyre.

For layers 4–7, according to Slawyk and Raimbault (1995), the nitrate released from dissolved organic nitrogen is at a rate of 0.0048–0.012 mmolN/m^3/day. If a water mass flows along the Kuroshio, it takes ~60 days from the KSJ to KKE (distance between the KSJ and KKE is ~1500 km, and the mean velocity of the Kuroshio in the intermediate layer is ~0.3 m/s). The product of the release rate and the duration of a water parcel flowing from the KSJ to KKE suggests that regeneration increases the nitrate concentration by a range of 0.3–0.7 mmolN/m^3. For vertical diffusive nitrate transport, assuming a mean upward nitrate flux of 10^{-6} mmolN/m^2/s (Kaneko et al., 2013), multiplying the duration of a water parcel flowing from the KSJ to KKE and dividing by the typical layer thickness of the intermediate layer (400 m), vertical diffusion increases the nitrate concentration by an order of 0.01 mmolN/m^3. Because net effective diffusion is the sum of the nitrate export through the upper interface and import through the lower interface, it should be less than 0.01 mmolN/m^3. The observed nitrate

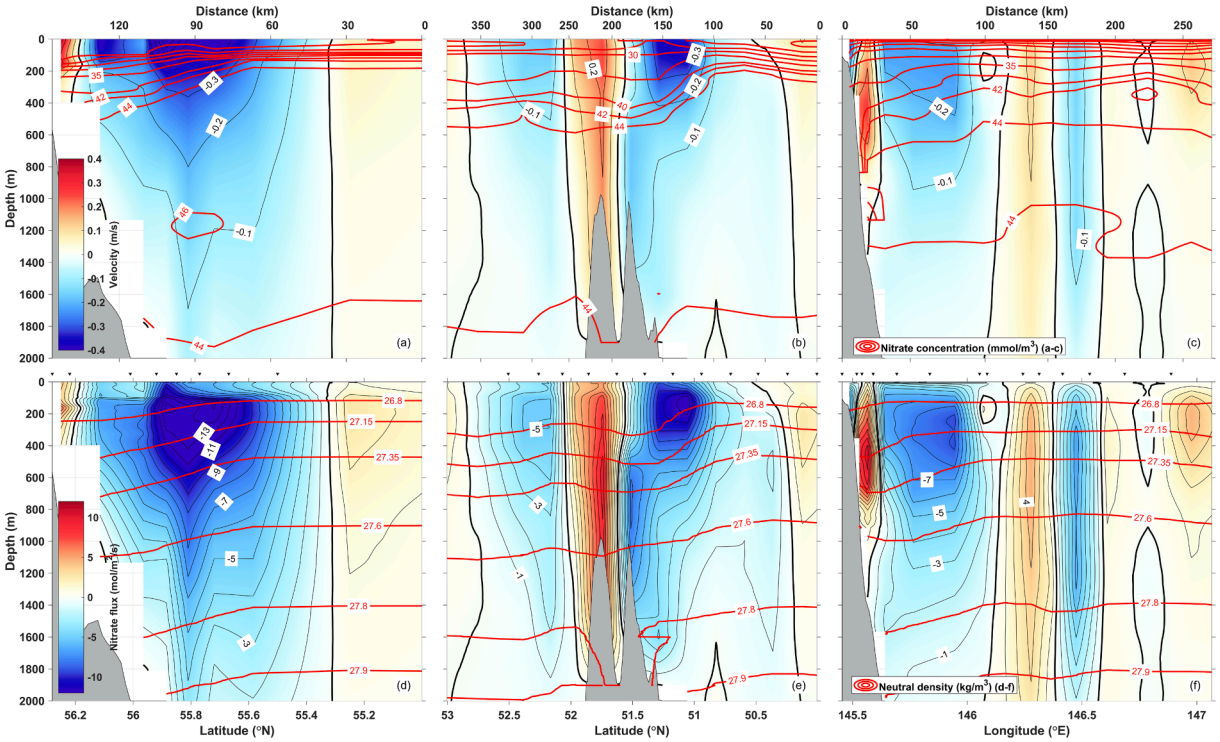

Fig. 6. Velocity and nitrate flux along the subarctic gyre. (a), (b), and (c) represent the eastern portion of the Alaskan Stream (at Section P16), the western portion of the Alaskan Stream (at Section P14), and the Oyashio (at Section P01). Red contours denote the nitrate concentration (mmol/m^3). (d), (e), and (f) represent the nitrate flux. Red contours denote the neutral density surface (kg/m^3) for the ASE, ASW, and OYA. Positive and negative values indicate eastward and westward directions, respectively.

Table 2
Volume transport (Vt), nitrate transport (Nt), transport weighted nitrate concentration (Ct) and area weighted nitrate concentration (Ca) of the Oyashio (at section P10), the Alaskan stream (West, at section P14), and the Alaskan stream (East, at section P16). Blue character denotes that the nitrate concentration decrease along the flow path. The lower boundary of the layers is 26.8, 27.15, 27.35, 27.6, 27.8, and 27.9 kg/m^3. Positive (negative) values indicate northward (southward) or eastward (westward).

	Vt (Sv)			Nt (kmol/s)			Ct (mmol/m^3)			Ca (mmol/m^3)		
	ASE	ASW	OYA	ASE	ASW	OYA	ASE	ASW	OYA	ASE	ASW	OYA
T	**−20.02**	**−19.05**	**−14.36**	**−788.12**	**−782.61**	**−577.62**	N/A	N/A	N/A	N/A	N/A	N/A
1–2	−5.11	−5.90	−2.00	−104.89	−183.52	−47.32	20.53	31.11	23.67	21.07	30.33	23.35
3	−3.65	−3.75	−3.31	−156.05	−158.62	−125.31	42.72	42.35	37.84	41.61	41.03	37.33
4	−3.33	−2.57	−2.97	−154.79	−120.47	−128.92	46.50	46.81	43.43	45.09	44.68	42.39
5	−3.91	−3.07	−2.79	−183.60	−144.89	−126.72	47.01	47.17	45.40	45.57	45.39	44.12
6	−2.78	−2.35	−2.41	−131.15	−110.43	−109.71	47.24	47.09	45.52	45.63	45.15	44.05
7	−1.25	−1.42	−0.88	−57.63	−64.69	−39.63	46.28	45.65	44.94	44.61	44.03	43.34

concentration increases from the KJS to KKE by 1.5, 2.1, 2.66, and 2.89 mmolN/m^3 for layers 4–7, respectively, and therefore, regeneration and diffusion are likely to be minor causes for the increase in nitrate concentration along the Kuroshio.

Although the diffusive nitrate flux contributes little to the increased nitrate concentration along the Kuroshio, it is important to the nitrate budget in the surface layer over the entire Kuroshio region. For example, with an assumption that a diffusive nitrate flux of 10^{-6}mmolN/m^2/s occurs over an area 2000 km long and 200 km wide, the upward diffusive nitrate supply is $\sim 13 \times 10^{12}$ molN/y.

5. Subarctic nutrient streams

The subarctic nutrient streams (Fig. 6) consist of the Alaskan Stream (ASE denotes the eastern section of the Alaskan Stream at Section P16, and ASW denotes the western section at P14, Fig. 1) and Oyashio (OYA at Section P1, Fig. 1). The Alaskan Stream flows along the Aleutian Island chain, enters the Bering Sea through several passes in the Aleutian Arc (Stabeno et al., 2005) and flows into the North Pacific through the Kamchatka Strait as the East Kamchatka Current. The East Kamchatka Current flows southward along the Kuril Island chain to the southeast of Hokkaido and is named the Oyashio. During the long journey, intense mixing along the island chain and water exchange with other water masses modifies the physical and biogeochemical properties of the ocean currents in the subarctic gyre.

In terms of the sectional velocity, there is a single surface maximum in the ASE (Fig. 6a). For the ASW (Fig. 6b), the eastward flow (Fig. 6b) is in the island wake and is treated together with the two adjacent westward flows when calculating volume and nitrate transport. The Oyashio (Fig. 6c) has four alternative flows with two northeastward and two southwestward flows. The left-most negative (southwestward) flow in the section is chosen to represent the Oyashio (Fig. 6c). The surface velocities of the ASE, ASW, and OYA are less than 0.4 m/s and decrease to a depth of 2000 m with the same sign. This structure results in large transport through the entire water column. The net volume transports over the upper 2000 m are 20.2, 19.1, and 14.4 Sv (Table 2) westward

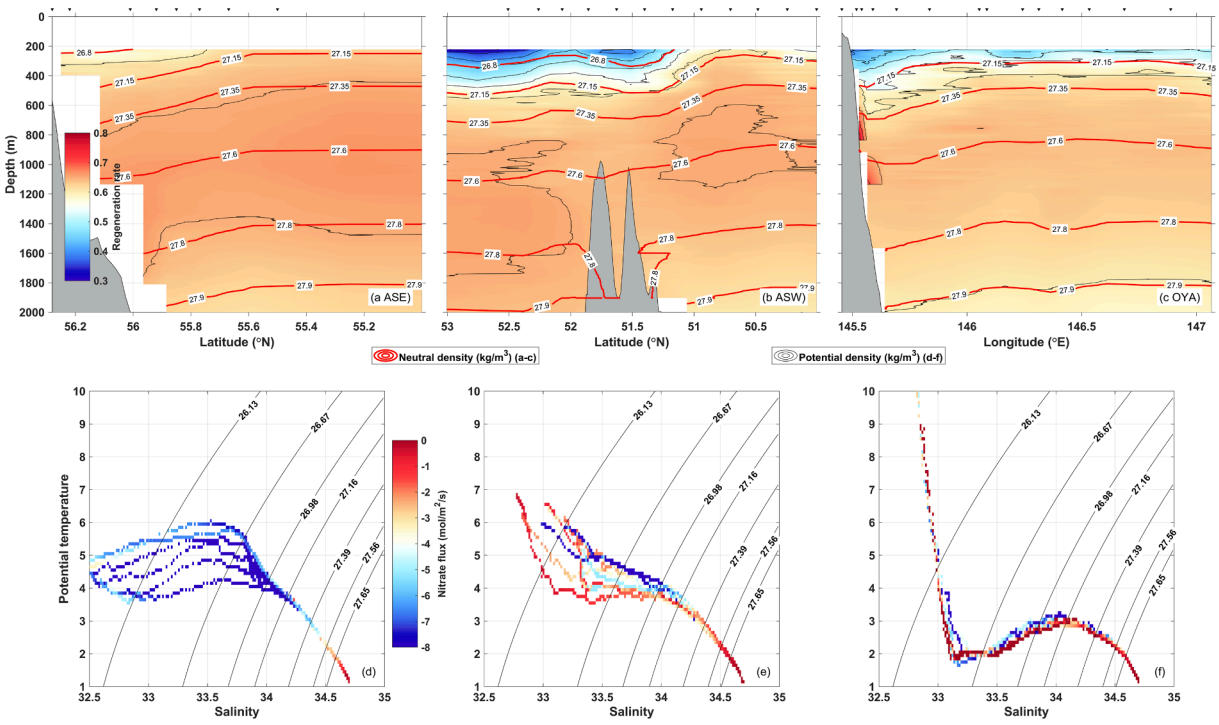

Fig. 7. (a), (b), and (c) represent the ratio of regenerated nitrate concentration to nitrate concentration of the eastern portion of the Alaskan Stream (at Section P16), the western portion of the Alaskan Stream (at Section P14), and the Oyashio. Red contours denote the neutral density surface (kg/m^3). The top layer is blank due to the large uncertainties. (d), (e), and (f) represent the temperature-salinity diagram, and color shading denotes the nitrate flux for the ASE, ASW, and OYA, respectively. Potential density contours 26.13, 26.67, 26.98, 27.16, 27.39, 27.56, and 27.65 in (d–f) correspond to neutral densities of 26.2, 26.8, 27.15, 27.35, 27.6, 27.8, and 27.9, respectively.

for the ASE, ASW, and OYA, respectively. The nitrate concentration reaches almost 15 mmolN/m^3 on the sea surface and increases to 40 mmolN/m^3 at a depth of 400 m. Therefore, the nutricline is stronger and shallower here than in the subtropical gyre.

The value of the nitrate flux subsurface maximum in three sections along the subarctic stream path (Fig. 6d–f) is comparable to that of the Kuroshio but is located at a shallower depth (200–300 m), showing the high possibility of carrying nutrients directly into the mixed layer. The nitrate transports for the ASE, ASW, and OYA are −788.1, −782.6, and −577.6 kmolN/s, respectively. The volume transport and nitrate transport between the ASE and ASW change little, while that from the ASW to OYA decreases. In contrast to the Kuroshio, there is no downstream intensification in volume transport and nitrate transport.

The nitrate concentration slightly decreases from the ASE to ASW (Table 2) in layers 3–7, and the reduction is evident from the ASW to OYA. Regeneration tends to increase the nitrate concentration along the nutrient stream, and therefore, it is not the candidate responsible for the reduced nitrate concentration. However, although there is strong tidal mixing along the Kuril and Aleutian island chains, the uniform reduction over several layers requires a net loss of nitrate in each individual layer; that is, the nitrate export at the upper interface is larger than the import at the lower interface (diffusive nitrate flux is upward according to the nitrate concentration gradient). Assuming an upper (lower) interface that has a large (small) diffusive nitrate flux of 10^{-5} (10^{-6}) mmolN/m^2/s (Kaneko et al., 2013), a typical horizontal velocity of 0.3 (0.2) m/s, a layer thickness of 300 m, and a distance between two sections of 2000 km, the nitrate concentration reduction reaches approximately 0.2 mmol/m^3 (10^{-5} mmolN/m^2/s × 2000 kmÃ·0.3 m/sÃ·300 m−10^{-6} mmolN/m^2/s × 2000 kmÃ·0.2 m/sÃ·300 m). This value is significantly smaller than the actual reduction (~1–2 mmol/m^3); therefore, we exclude the possibility of regeneration and vertical diffusion. The lateral water exchange is left and will be examined in detail.

To determine what occurs from the ASE to OYA, the change in water mass using a T-S diagram is presented (Fig. 7). The T-S relationship (Fig. 7d–f) shows that from the ASE to ASW, the water mass property changes little, while from the ASW to OYA, the core of the nutrient stream, where the subsurface maximum of nitrate flux is located, becomes cooler. The isopycnal range of the subsurface nutrient flux maximum (Fig. 6d–f) scarcely changes along the nutrient stream, and therefore, this subsurface cooling simply implies the existence of lateral water exchange with cold water. Therefore, when considering the reduction in nitrate concentration along the subarctic gyre, the candidate involved in the lateral exchange process should have low temperatures and/or low nitrate concentrations.

From the ASE to ASW, there is net northward transport through the southern boundary of the box (Box 10 in Fig. 1) (Fig. 2). The seawater is from lower latitudes and therefore has a lower nitrate concentration. It merges into the westward Alaskan Stream and flows out of the box through its western boundary. The lateral water exchange with the low nitrate concentration seawater from the south is the cause of the reduction of nitrate concentration from the ASE to ASW. Moreover, layers 4–6 of the ASE and ASW are deeper than 500 m (Fig. 6d–f), while the passes in the Aleutian Island chain (northern boundary of Box 10) are shallower than 500 m, and water exchange with the southern area is therefore the only cause in these layers.

From the ASW to OYA, the situation is complicated because the Bering Sea and Okhotsk Sea can both affect the nitrate concentration along the stream path. The ASW section is located in the upstream region where the water exchange between the Alaskan Stream and Bering Sea occurs, and the OYA section is in the downstream region where water exchange between the East Kamchatka Current and Okhotsk Sea occurs. Roden (1995) demonstrated that the nutrient concentration (silicate, nitrate, and phosphate) of deep water is higher in the Bering Sea than in the North Pacific. Therefore, water exchange with or water input from the Bering Sea increases the nitrate concentration along the stream path. Andreev et al. (2010) demonstrated that the Okhotsk Sea receives 1.0 ×

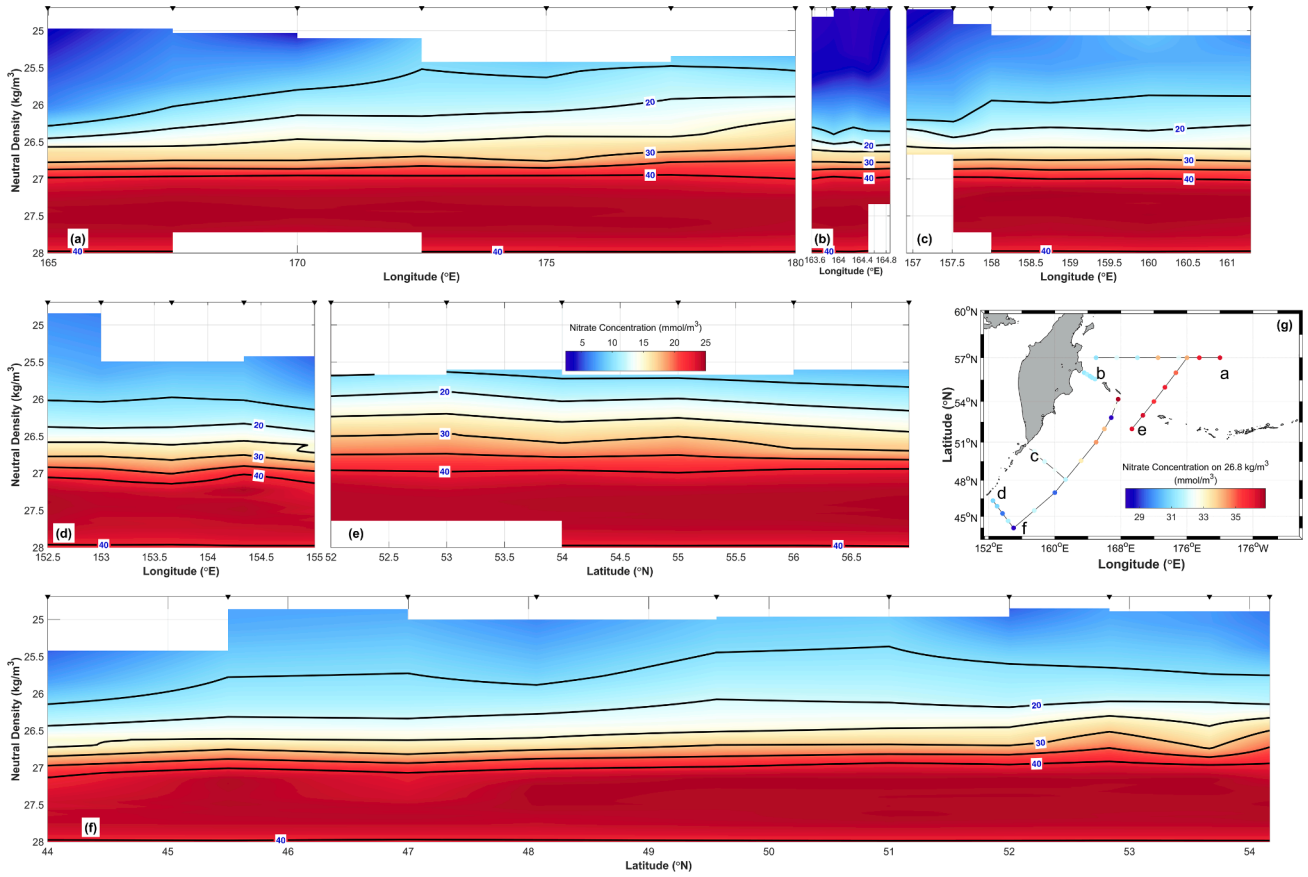

Fig. 8. Nitrate concentration as a function of neutral density and longitude/latitude at several sections in the Bering Sea and in the East Kamchatka Current. Location of the sections (a)–(f) is given in (g). The color scales in (a)–(f) are different from those in (g).

10^{12} dissolved inorganic nitrogen, 4.0×10^{10} dissolved inorganic phosphorus, and 4.0×10^{12} dissolved inorganic carbon annually from the North Pacific. Their estimation was apparently based on a water exchange of 3–5 Sv and the nutrient concentration difference between the Okhotsk Sea and North Pacific, that is, the effective transport. Nishioka et al. (2020) reported that the upward nitrate transport around the Kuril Island chain was 0.19×10^{12} molN/y, while that around the Aleutian Island chain was 0.09×10^{12} molN/y. The upward nitrate transport was smaller than the nitrate export from the North Pacific to the Okhotsk Sea. The hydrographic profiles in the Okhotsk Sea, obtained from the Japan Meteorological Agency (JMA), and the Bering Sea, obtained from JAMSTEC, were used to explain the nitrate concentration variation from the ASW to OYA.

Although the Bering Sea is considered to be a nutrient source, particularly for silica, to the North Pacific, its nutrient export is rarely discussed because of the lack of data. Therefore, the MR080500 and MR040400 cruises from JAMSTEC were chosen to illustrate the spatial variation in the nutrient concentration from the Bering Sea to the North Pacific. The nitrate concentration in the Bering Sea, especially in the Aleutian Basin (Line a, Fig. 8), is higher than that in the downstream region of the East Kamchatka Current (Line d, Fig. 8). The upper layer shows an undulated contour of nitrate concentration along the section (Fig. 8f), which is depressed in the Kamchatka Strait (Fig. 8b) and uplifted in its downstream region (Fig. 8c–d). In a density layer of 26.8 kg/m^3, the nitrate concentration in the Bering Sea exceeds that in the North Pacific by ~4 mmolN/m^3 (Fig. 8g). Because the volume transport of the East Kamchatka Current is ~10 Sv (Panteleev et al., 2006), the effective nitrate transport (Ayers et al., 2014) from the Bering Sea to the North Pacific should be on the order of 1.3×10^{12} molN/y. This value is comparable to the nitrate transport from the North Pacific to the Okhotsk Sea (Andreev et al., 2010) and is larger than the upward nitrate transport around the island chains.

The North Pacific has a higher nitrate concentration than the Okhotsk Sea in the same isopycnal layer, particularly in the intermediate layer (26.13–26.98 kg/m^3, Fig. 9b, c). The nitrate concentration, as a function of depth (Fig. 9e) or potential density (Fig. 9g), shows that there is a reduced nitrate concentration from north to south in the North Pacific. The nitrate concentration is higher in a latitude band of 48–50°N in the North Pacific (Fig. 9e) than in the Okhotsk Sea in the upper 1000 m (Fig. 9d) and is similar to that in the Okhotsk Sea when reaching a latitude band of 41–42°N. Because the Oyashio water on the Pacific side moves from high latitudes to low latitudes, the reduction in nitrate concentration during its movement from 48–50°N to 41–42°N indicates the possibility that Okhotsk Sea water with a low nitrate concentration is mixed with Oyashio water.

The nutrient stream in the subarctic gyre has comparable nutrient transport as that in the subtropical gyre but has a shallower subsurface maximum. Its nitrate concentration decreases along the stream path. Although other mechanisms, such as vertical mixing and biogeochemical processes, may affect the nitrate concentration, this reduction is mainly due to lateral water exchange. The Bering Sea and Okhotsk Sea act as sources and sinks, respectively, for nutrients carried by the nutrient stream in the subarctic gyre.

6. Other nutrient transfers

The vertical nitrate transfer derived from the inverse method consists of two components: vertical advection and vertical diffusion. Although the vertical velocity derived from the inverse calculation may be affected by the initial imbalance (net transport integrated along the sections that encloses a box) within each layer of the box, the value of vertical volume transport still meets our general knowledge on the order

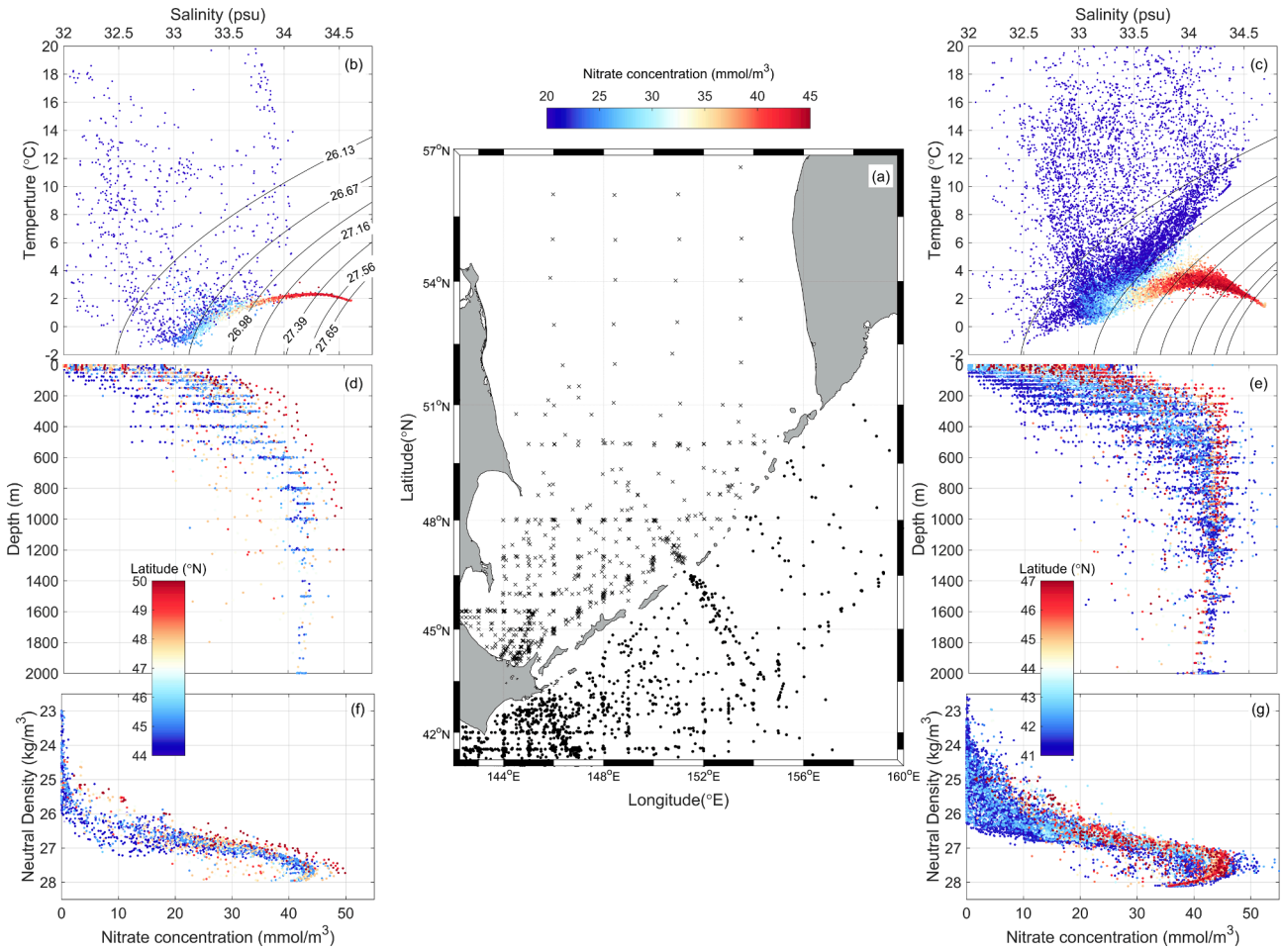

Fig. 9. Comparison of nitrate concentrations between the Okhotsk Sea and North Pacific. (a) Locations of the hydrographic casts. Crosses and dots indicate the hydrographic casts in the Okhotsk Sea and North Pacific. The left and right panels are for the Okhotsk Sea (b, d, f) and North Pacific (c, e, g), respectively. (b) and (c) are the T-S diagrams with color showing nitrate concentration. (d) and (e) are the nitrate concentration as a function of depth with color showing latitude. (f) and (g) show the nitrate concentration as a function of neutral density, with color showing latitude. Potential density contours 26.13, 26.67, 26.98, 27.16, 27.39, 27.56, and 27.65 in (b, c) correspond to neutral densities of 26.2, 26.8, 27.15, 27.35, 27.6, 27.8, and 27.9, respectively.

of magnitude, as does nitrate transport. According to the results presented here (Table 3) (further details provided in the Appendix), the vertical diffusive nitrate transport is positive at the lower interface of layers 1–5 due to the positive vertical gradient of nitrate concentration (Fig. 4) and negative at the lower interface of layers 6–7 due to the negative vertical gradient of nitrate concentration (Fig. 6).

Vertical nitrate transport provides information on the nutrient budget in the North Pacific. Nishioka et al. (2020) suggested that vertical diffusion supplies nitrate from the subarctic intermediate nutrient pool to the upper layer at a rate of 0.1–10 $\times$ 10^{12} molN/y. They further mentioned that nitrate transport from the deep layer to the intermediate layer is unclear. Using the inverse calculation, a general estimation of these two nitrate transports can be given. First, nitrate import from the Bering Sea (1 $\times$ 10^{12} molN/y, this study), nitrate export to the Okhotsk Sea (1 $\times$ 10^{12} molN/y, Andreev and Pavlova, 2010), and nitrate export to the subtropical gyre through NPIW formation (0.76 $\times$ 10^{12} molN/y, Long et al., 2019) suggest a net nitrate export of 0.76 $\times$ 10^{12} molN/y. Second, the subarctic intermediate nutrient pool is within a potential density range of 26.6–27.5 kg/m^3, which corresponds to a neutral density range of 26.7–27.7 kg/m^3. Taking a neutral density of 26.8 kg/m^3 and 27.6 kg/m^3 as an approximation of the subarctic intermediate nutrient pool and using the northern half of Boxes 6, 7, and 8 (sum of half of the vertical nitrate transport in Boxes 6, 7, and 8) and all of Boxes 9, 10, and 11 (sum of the vertical nitrate transport in Boxes 9, 10, and 11) to represent the area of the subarctic intermediate nutrient pool, the nitrate transport from the intermediate layer to the upper layer is 1.31 $\times$ 10^{12} molN/y (Table 3) (=(24.8 + 10.24 + 12.08)/2 + 2–16.29 + 32.37 kmolN/s), and from the deep layer to the intermediate layer it is 0.27 $\times$ 10^{12} molN/y (Table 3) (=(−17.98 + 2.89–5.77)/2 + 1.64 + 23.66–6.39 kmolN/m^3). The vertical nitrate transport derived from the inverse calculation of this study gives a deficit of 1.04 $\times$ 10^{12} molN/y (=1.31 $\times$ 10^{12} – 0.27 $\times$ 10^{12} molN/y). Third, Nishioka et al. (2020) estimated that nitrate export from the surface to depth was 1.79–2.76 $\times$ 10^{12} molN/y. Hence, the nitrate export from the bottom of the intermediate layer to the depth should be within a range of 0–0.96 $\times$ 10^{12} molN/y (1.79–2.76 $\times$ 10^{12}–1.04 $\times$ 10^{12}–0.76 $\times$ 10^{12} molN/y).

Subduction and induction processes can transport nutrients between the mixed layer and permanent thermocline. These processes provide routes for the exchange between the nutrient-depleted surface layer and nutrient-rich subsurface layer. Williams et al. (2006) demonstrated that the Gulf Stream nutrient stream contributes 40% to the nitrate transport provided by the induction process. This value is still unknown in the North Pacific. Referring to the subduction amount given by Qiu and Huang (1995), nutrient transport by this process can be approximately estimated. The volume transport induced by subduction and induction are 32.5 and 7.8 Sv, respectively, in terms of annual mean (Qiu and Huang, 1995). The nitrate concentration in the subduction water can be 5 mmol/m^3 (this value is from the first layer in Table 1, to represent the surface layer of the subtropical gyre), while that in induction water is 21 mmol/m^3 (this value is from the first layer in Table 2, to represent the

Table 3
Vertical advective (w), diffusive (d) and vertical (v, sum of w and d) nitrate transport (kmolN/s) within each box. The locations of the boxes are shown in Fig. 1. Positive values indicate upward.

		BOX1	BOX2	BOX3	BOX4	BOX5	BOX6	BOX7	BOX8	BOX9	BOX10	BOX11
26.20	**w**	−9.81	−19.49	18.88	−0.19	8.42	29.57	−6.41	−4.72	N/A	N/A	N/A
	d	7.39	4.60	7.58	10.14	8.63	21.01	8.08	16.63	N/A	N/A	N/A
	v	−2.42	−14.89	26.46	9.95	17.05	50.58	1.68	11.91	N/A	N/A	N/A
26.80	**w**	7.70	−15.58	−0.03	−4.95	−12.85	13.06	−1.44	3.02	−10.67	−29.37	1.80
	d	8.03	9.57	9.50	8.03	6.95	11.75	11.68	9.06	12.67	13.08	30.57
	v	15.73	−6.00	9.47	3.08	−5.90	24.80	10.24	12.08	2.00	−16.29	32.37
27.15	**w**	18.23	−19.49	−16.32	−4.49	−22.05	8.28	−4.44	4.09	5.86	−18.43	−9.80
	d	4.06	5.01	4.68	2.65	3.30	2.97	4.17	2.83	1.74	1.77	3.32
	v	22.29	−14.48	−11.64	−1.84	−18.75	11.25	−0.27	6.92	7.60	−16.67	−6.48
27.35	**w**	−13.85	−13.35	−28.55	−5.24	−12.85	4.08	−1.99	0.80	−0.27	4.39	−24.20
	d	1.79	1.74	1.06	0.77	1.49	0.92	1.26	0.86	0.38	0.44	0.27
	v	−12.06	−11.60	−27.50	−4.48	−11.37	5.00	−0.72	1.66	0.11	4.83	−23.93
27.60	**w**	8.89	6.51	−48.49	15.47	11.95	−18.13	2.81	−5.77	1.49	23.58	−6.35
	d	0.14	0.08	−0.16	−0.13	0.29	0.16	0.07	0.00	0.15	0.08	−0.04
	v	9.03	6.59	−48.65	15.34	12.24	−17.98	2.89	−5.77	1.64	23.66	−6.39
27.80	**w**	2.29	31.93	−31.69	15.22	−6.93	−20.89	−1.63	−8.94	1.89	4.52	−0.08
	d	−0.34	−0.31	−0.28	−0.27	−0.23	−0.19	−0.27	−0.29	−0.29	−0.19	−0.28
	v	1.95	31.62	−31.98	14.95	−7.16	−21.08	−1.90	−9.23	1.60	4.34	−0.36
27.90	**w**	−0.22	35.92	−4.28	−8.57	−13.42	−13.60	−6.85	−3.32	0.03	−13.62	10.84
	d	−0.34	−0.42	−0.31	−0.31	−0.35	−0.40	−0.34	−0.37	−0.35	−0.32	−0.38
	v	−0.57	35.50	−4.59	−8.88	−13.76	−14.00	−7.19	−3.68	−0.32	−13.94	10.45

surface layer of the subarctic gyre). Their net effect can be defined as the ventilation process that contributes approximately 163 kmolN/s (=5.17 $\times 10^{12}$ molN/y, from the mixed layer to the permanent thermocline) and 164 kmolN/s (=5.17 $\times 10^{12}$ molN/y, from permanent thermocline to mixed layer), respectively. These values are almost twice that of the vertical nitrate transport derived from the inverse calculation at the lower interface of the top layer (26.2 kg/m^3, 100 kmolN/s or 3.15 $\times 10^{12}$ molN/y, upward, 84 kmolN/s for vertical diffusion and 16 kmolN/s for vertical advection) (Table 3, Row 4), although only half of the subtropical gyre was included in this calculation. Consequently, subduction and induction processes play an essential role in the nitrate budget in the upper layer of the North Pacific.

7. Concluding remarks

By applying the inverse method, the absolute geostrophic velocity normal to the WOCE-revisit sections was calculated. The nitrate flux was determined by multiplying the velocity and nitrate concentration and was integrated over the section to obtain the nitrate transport. The spatial pattern of the volume transport and nitrate transport per unit width was presented for four isopycnal layers. The spatial pattern showed that the upper portion of the nutrient transport was related to the mode waters and recirculation in the subtropical gyre, while the intermediate portion was closely related to the distribution of the NPIW and had the most intensive nutrient transport.

The nutrient streams of the Kuroshio, the Alaskan Stream, and Oyashio drive the most intensive nutrient transport within the basin. Both the volume transport and nitrate transport of the Kuroshio are increased downstream, which is due to the Kuroshio recirculation gyre. The nitrate concentration in the same isopycnal layers increases along the Kuroshio path. This variation from the area south of Japan to the Kuroshio Extension is due to the confluence of the high nitrate concentration water from the north.

For the subarctic gyre, there is no downstream intensification in the volume and nitrate transport from the Alaskan Stream to the Oyashio. The nitrate concentration decreases within most layers along the subarctic gyre. The lateral water exchange with the relatively low latitude area and the Okhotsk Sea decreases the nitrate concentration along the nutrient stream in the subarctic gyre. The biogeochemical processes and vertical diffusion play a minor role in the change in nitrate concentration along the stream path.

The contribution of vertical nitrate transport to the subarctic intermediate nutrient pool was estimated. The ventilation processes, in which the subduction that carries nutrients from the mixed layer to the permanent thermocline in the subtropical gyre (5.17 $\times 10^{12}$ molN/y) and induction that carries nutrients from the permanent thermocline to the mixed layer in the subarctic gyre (5.17 $\times 10^{12}$ molN/y) are comparable to the sum of dianeutral and diffusive nutrient transport (3.15 $\times 10^{12}$ molN/y). The results of this study confirm that vertical nitrate transport is important at the basin scale and that lateral water exchange with adjacent seawater is responsible for the change in nitrate transport and nitrate concentration along the nutrient streams in the North Pacific. This analysis is based on the steady state and lacks temporal information; therefore, the ventilation processes should be quantified using a physical-biogeochemical coupled model in future work.

Declaration of Competing Interest

The authors declare that they have no known competing financial interests or personal relationships that could have appeared to influence the work reported in this paper.

Acknowledgments

This study was supported by the National Natural Science Foundation of China (42106035, 41920104006), Scientific Research Fund of Second Institute of Oceanography, MNR (grants JB2105 and JZ2001), the China Postdoctoral Science Foundation (grant 2020M681969), the Innovation Group Project of the Southern Marine Science and Engineering Guang dong Laboratory, Zhuhai (No. 311020004), and the grants from the Ministry of Education, Culture, Sports, Science and Technology, Japan (MEXT) to a project on Joint Usage/Research Center— Leading Academia in Marine and Environmental research (LaMer). X. Guo thanks support by JSPS KAKENHI (grant numbers 20H01972) and by the Environment Research and Technology Development Fund JPMEERF20205005 of the Environmental Restoration and Conservation Agency of Japan. The data used in this study were from CCHDO (https://cchdo.ucsd.edu/), CCMP (http://www.remss.com/measureme

nts/ccmp/), ECMWF (https://www.ecmwf.int/) and WOA (https://www.nodc.noaa.gov/OC5/woa13/). The authors appreciate the scientists and crews who deploy the WOCE-revisit cruise. The authors appreciate Dr. J.L. Pelegrí and another anonymous reviewer and Dr. Shin-ichi Ito for their supportive comments on the original manuscript.

Appendix

The WOCE data from 2004 to 2007 were used in the inverse calculation. Generally, the available hydrographic data encompass the period from 1985 to the present. This period was chosen to reduce temporal aliasing error due to decadal oceanic variations in the North Pacific (e.g., Pacific Decadal Oscillation, North Pacific Gyre Oscillation, and Kuroshio Extension Decadal Oscillation). In addition, the stations were carefully chosen to avoid large transient variations at the hydrographic line intersections, as suggested by Macdonald et al. (2009). This is because if part of the eddy was sampled at the endpoints of the section, this may induce an error to the baroclinic structure (it is dependent on water depth) in the initial imbalance of property within the box. Although the vertical velocity and diffusion may be affected by this initial error, the reference velocity is not sensitive.

Apart from the WOCE data, other datasets were also used in the inverse calculation. The Ekman transport was calculated from the CCMP wind product (0.25° × 0.25°) (2004–2007), and sea surface freshwater flux (evaporation-precipitation) was calculated from the European Center for Medium-Range Weather Forecasts (ECMWF) ERA-interim reanalysis data (0.25° × 0.25°) (2004–2007). The density, salinity, and concentrations of silicate and nitrate for calculating the Ekman mass, silicate transport and neutral density surface were determined using WOA13 (World Ocean Atlas, 2013) version 2 data.

The inverse box model (Wunsch, 1978) assumes conservation of mass, salt, P* (170P + O), heat, and silicate in each individual layer separated by a neutral density surface of 26.2, 26.8, 27.15, 27.35, 27.6, 27.8, 27.9, 27.95, 28, 28.05, 28.09, 28.1, and 28.11 kg/m^3 for boxes south of Section P1, while of 26.8, 27.15, 27.35, 27.6, 27.8, 27.9, 27.95, 28, 28.05, 28.09, 28.1, and 28.11 kg/m^3 for the remaining boxes to avoid outcropping in the box. Their selection follows the definition of the vertical boundary of the water mass (Macdonald et al., 2009; Ganachaud and Wunsch, 2002) or the entire water column (Table A1). By using the thermal wind relation, the geostrophic velocity referring to the 28.05 kg/m^3 neutral density layer (at a depth of approximately 3000 m) is calculated.

The general form of the equation is:

$$\sum_{\mathrm{m}}\sum_{\mathrm{i}}\sum_{\mathrm{j=U}}^{\mathrm{L}} a_{\mathrm{mi}}\mathbf{v}_{\boldsymbol{R}\mathrm{mi}}C_{\mathrm{mij}} - \mathbf{w}_{\mathrm{U}}\alpha_{\mathrm{U}}C_{b\mathrm{U}} + \mathbf{w}_{\mathbf{L}}\alpha_{\mathrm{L}}C_{b\mathrm{L}} + \kappa_{\mathbf{Z}_{\mathrm{U}}}\alpha_{\mathrm{U}}\left(\frac{\partial C_{b\mathrm{L}}}{\partial Z}\right) + \kappa_{\mathbf{Z}_{\mathbf{L}}}\alpha_{\mathrm{L}}\left(\frac{\partial C_{b\mathrm{L}}}{\partial Z}\right) - \sum_{\mathrm{m}}\mathbf{E}_{\mathbf{m}}\sum_{\mathrm{i}}V_{EK\,\mathrm{mi}}C_{surf\,\mathrm{mi}} + \mathbf{FW} \approx -\sum_{\mathrm{m}}\sum_{\mathrm{i}}\sum_{\mathrm{j}} a_{\mathrm{mij}}v_{G\mathrm{mij}}C_{\mathrm{mij}}. \tag{A1}$$

The bold characters are the unknowns. $\mathbf{V}_{\boldsymbol{R}}$ denotes the velocity at the reference level, $\mathbf{w}$ denotes the vertical velocity, κ_z denotes the eddy diffusivity, $\mathbf{E}_{\boldsymbol{m}}$ is the Ekman component correction factor, and **FW** is the fresh water flux.

C represents concentrations at each 1 dbar level (2 dbar interval data were linearly interpolated to a 1 dbar interval). Subscripts i, j, and m denote the indices of the station pairs, indices of one level within each layer, and each side (usually the subsection) of the box, respectively. Specifically, C is ρ for mass, α represents the interface areas and is calculated from the World Ocean Atlas, a represents the distance of each station pair, C_b represents concentrations at the boundary of each interface as derived from the in situ sectional data, and U and L denote the upper and lower boundaries of the layer, respectively. V_{EK} is the Ekman volume transport and is calculated from the CCMP wind product and the WOA surface density, C_{surf} is the concentration (ρ and nutrient concentration) at the sea surface and is derived from the WOA data, and V_G denotes the baroclinic velocity calculated by the thermal wind relation.

For the terms on the left-hand side, the first term denotes the relative transport, the second and third terms denote the vertical transport through the upper and lower interface of an individual layer, the fourth and fifth terms denote the vertical diffusion through the upper and lower interfaces of an individual layer, and the sixth and seventh terms denote the Ekman transport and fresh water transport, respectively. The right-hand side represents the initial imbalance of the properties.

The Guass-Markov estimator was used to solve the underdetermined problem (because the amount of velocity within station pairs usually exceeds that of constraints, the number of unknowns exceeds the number of equations). All conservation equations were weighted according to their a priori uncertainties. Compared to the tapered-weighted least squares, this solves the part of the solution that is not resolved by the constraints. The first guess of the solution, or the a priori information, is as follows: 0.2 m/s, 0.05 m/s, and 0.02 m/s for the depth of a station pair shallower than 500 m, from 500 to 1000 m and deeper than 1000 m, respectively; 1×10^{-6} m/s and 10^{-4} m^2/s for dianeutral velocity and eddy diffusivity, respectively; and the coefficient of variation (standard deviation/mean, during 2004–2007) of Ekman transport at each subsection for Ekman correction, EP (sum of evaporation (upward, negative) and total precipitation (downward, positive)), in each box for the EP correction. A priori noise is set as 0.5×10^9 kg/s for mass in each individual layer that is not in contact with the sea surface and 1×10^9 kg/s for the surface layer and the entire water column. For the salinity anomaly, PO (170 phosphate + oxygen) anomaly, and heat anomaly, a priori is set to be the standard deviation of the corresponding variable in each layer multiplied by 4×10^9. The a priori for silicate is set as 52×10^9.

According to the interpretation of the inverse results, this represents the mean state of the large-scale circulation during 2004–2007. Four out of

Table A1
Size of matrix of each term in the inverse problem as defined by Equation (A1). Abbreviations: SP for station pairs, IL for individual layers, Bo for boxes, SuB for subsections, and N/A for not applicable. The property transport of the water column means the integration over full water depth, the lower layers means the layers that do not contact the sea surface.

	Relative transport	Dianeutral transport	Diffusion	Ekman correction	E-P correction
Mass	151 IL × 674 SP	151 IL × 140 IL	N/A	151 IL × 20 SuB	151 IL × 11 Bo
Mass for water column	11 Bo × 674 SP	11 Bo × 140 IL	N/A	11 Bo × 20 SuB	11 Bo × 11 Bo
Salt anomaly for lower layers	140 IL × 674 SP	140 IL × 140 IL	140 IL × 140 IL	N/A	N/A
Salt for water column	11 Bo × 674 SP	11 Bo × 140 IL	11 Bo × 140 IL	11 Bo × 20 SuB	N/A
PO anomaly for lower layers	140 IL × 674 SP	140 IL × 140 IL	140 IL × 140 IL	N/A	N/A
Heat anomaly for lower layers	140 IL × 674 SP	140 IL × 140 IL	140 IL × 140 IL	N/A	N/A
Silicate for water column	11 Bo × 674 SP	11 Bo × 140 IL	11 Bo × 140 IL	11 Bo × 20 SuB	N/A

604 (less than 1%) solutions exceed the a priori mentioned above, indicating that the results are well constrained by the a priori. The spatial pattern of deep flow, net volume, heat, and mass transport over transoceanic sections such as P1, P2, and P3 were validated by comparison with those reported in Mcdonald et al. (2009), Roemmich and McCallister (1989), and Ganachaud and Wunsch (2002).

References

Andreev, A.G., Pavlova, G.Y., 2010. Marginal seas: Okhotsk Sea. In: Liu, K.K. (Ed.), Carbon and Nutrient Fluxes in Continental Margins. Springer, Berlin, Heidelberg, p. 394.

Ayers, J.M., Strutton, P.G., Coles, V.J., Hood, R.R., Matear, R.J., 2014. Indonesian throughflow nutrient fluxes and their potential impact on Indian Ocean productivity. Geophys. Res. Lett. 41 (14), 5060–5067. https://doi.org/10.1002/2014GL060593.

Chen, C.T.A., Liu, C.T., Pai, S.C., 1994. Transport of oxygen, nutrients and carbonates by the Kuroshio current. Chin. J. Oceanol. Limnol. 12 (3), 220–227. https://doi.org/10.1007/BF02845167.

Csanady, G.T., 1990. Physical basis of coastal productivity. The SEEP and MASAR experiments. EOS Trans. Am. Geophys. Union 71 (36), 1060. https://doi.org/10.1029/EO071i036p01060.

Ganachaud, A., Wunsch, C., 2002. Oceanic nutrient and oxygen transports and bounds on export production during the World Ocean Circulation Experiment. Global Biogeochem. Cycles 16 (4), 5-1–5-14.

Gordon, A.L., Ffield, A., Ilahude, A.G., 1994. Thermocline of the Flores and Banda seas. J. Geophys. Res. 99 (C9), 18235–18242. https://doi.org/10.1029/94JC01434.

Guo, X., Zhu, X.-H., Long, Y., Huang, D., 2013. Spatial variations in the Kuroshio nutrient transport from the East China Sea to south of Japan. Biogeosci. Discuss. 10 (4), 6737–6762. https://doi.org/10.5194/bgd-10-6737-2013.

Guo, X., Zhu, X.-H., Wu, Q., Huang, D., 2012. The Kuroshio nutrient stream and its temporal variation in the East China Sea. J. Geophys. Res. 117, C01026. https://doi.org/10.1029/2011JC007292.

Kaneko, H., Yasuda, I., Komatsu, K., Itoh, S., 2013. Observations of vertical turbulent nitrate flux across the Kuroshio. Geophys. Res. Lett. 40 (12), 3123–3127. https://doi.org/10.1002/grl.50613.

Letscher, R.T., Primeau, F., Moore, J.K., 2016. Nutrient budgets in the subtropical ocean gyres dominated by lateral transport. Nat. Geosci. 9 (11), 815–819. https://doi.org/10.1038/ngeo2812.

Long, Y.u., Zhu, X.-H., Guo, X., Huang, H., 2018. Temporal variation of Kuroshio nutrient stream south of Japan. J. Geophys. Res. Oceans 123 (11), 7896–7913. https://doi.org/10.1029/2017JC013635.

Long, Y.u., Zhu, X.-H., Guo, X., 2019. The Oyashio nutrient stream and its nutrient transport to the mixed water region. Geophys. Res. Lett. 46 (3), 1513–1520. https://doi.org/10.1029/2018GL081497.

Lozier, M.S., Dave, A.C., Palter, J.B., Gerber, L.M., Barber, R.T., 2011. On the relationship between stratification and primary productivity in the North Atlantic. Geophys. Res. Lett. 38, L18609. https://doi.org/10.1029/2011GL049414.

Macdonald, A.M., Mecking, S., Robbins, P.E., Toole, J.M., Johnson, G.C., Talley, L., Cook, M., Wijffels, S.E., 2009. The WOCE-era 3-D Pacific Ocean circulation and heat budget. Prog. Oceanogr. 82 (4), 281–325.

Nishioka, J., Nakatsuka, T., Watanabe, Y.W., Yasuda, I., Kuma, K., Ogawa, H., Ebuchi, N., Scherbinin, A., Volkov, Y.N., Shiraiwa, T., Wakatsuchi, M., 2013. Intensive mixing along an island chain controls oceanic biogeochemical cycles. Global Biogeochem. Cycles 27 (3), 920–929. https://doi.org/10.1002/gbc.20088.

Nishioka, J., Obata, H., Ogawa, H., Ono, K., Yamashita, Y., Lee, K., Takeda, S., Yasuda, I., 2020. Subpolar marginal seas fuel the north pacific through the intermediate water at the termination of the global ocean circulation. Proc. Natl. Acad. Sci. 117 (23), 12665–12673.

Palter, J.B., Lozier, M.S., Barber, R.T., 2005. The effect of advection on the nutrient reservoir in the North Atlantic subtropical gyre. Nature 437 (7059), 687–692. https://doi.org/10.1038/nature03969.

Palter, J.B., Lozier, M.S., 2008. On the source of Gulf Stream nutrients. J. Geophys. Res. 113, C06018. https://doi.org/10.1029/2007JC004611.

Panteleev, G.G., Stabeno, P., Luchin, V.A., Nechaev, D.A., Ikeda, M., 2006. Summer transport estimates of the Kamchatka Current derived as a variational inverse of hydrophysical and surface drifter data. Geophys. Res. Lett. 33, L09609. https://doi.org/10.1029/2005GL024974.

Pelegri, J.L., Csanady, G.T., 1991. Nutrient transport and mixing in the gulf stream. J. Geophys. Res. 96 (C2), 2577–2583. https://doi.org/10.1029/90JC02535.

Pelegrí, J.L., Csanady, G.T., Martins, A., 1996. The North Atlantic nutrient stream. J. Oceanogr. 52 (3), 275–299.

Pelegrí, J.L., Marrero-Díaz, A., Ratsimandresey, A.W., 2006. Nutrient irrigation of the North Atlantic. Prog. Oceanogr. 70 (2-4), 366–406.

Pelegrí, J.L., Vallès-Casanova, I., Orúe-Echeverría, O., 2019. The Gulf Nutrient Stream. In: Nagai, T., Saito, H., Suzuki, K., Takahashi, M. (Eds.), Kuroshio Current: Physical, Biogeochemical and Ecosystem Dynamics, GMS 243. AGU-Wiley, pp. 23–50. ISBN 9781119428343.

Qiu, B.O., Chen, S., 2006. Decadal variability in the formation of the north pacific subtropical mode water: oceanic versus atmospheric control. J. Phys. Oceanogr. 36 (7), 559–568.

Qiu, B., Huang, R.X., 1995. Ventilation of the North Atlantic and North Pacific : subduction versus obduction. J. Phys. Oceanogr. 25 (10), 2374–2390. https://doi.org/10.1175/1520-0485(1995)025<2374:VOTNAA>2.0.CO;2.

Redfield, A.C., Ketchum, B.H., Richards, F.A., 1963. The influence of organisms on the composition of sea-water. Symposium on experimental and efficient algorithms. In: Hill, M.N. (Ed.), The Sea, Vol. 2. Wiley-Interscience, New York, pp. 26–77.

Roden, G.I., 1995. Aleutian Basin of the Bering Sea:Thermohaline, oxygen, nutrient, and current structure in July 1993. J. Geophys. Res. 100, 13539–13554.

Roemmich, D., McCallister, T., 1989. Large scale circulation of the North Pacific Ocean. Prog. Oceanogr. 22 (2), 171–204.

Sarmiento, J.L., Gruber, N., 2006. Ocean Biogeochemical Dynamics. Princeton University Press, Princeton, N. J.

Sarmiento, J.L., Gruber, N., Brzezinski, M.A., Dunne, J.P., 2004. High-latitude controls of thermocline nutrients and low latitude biological productivity. Nature 427 (6969), 56–60. https://doi.org/10.1038/nature02127.

Slawyk, G., Raimbault, P., 1995. A simple procedure for simultaneous recovery of dissolved inorganic and organic nitrogen in lSN-tracer experiments and improving the isotopic mass balance. Mar. Ecol. Pro & Set. 124, 289–299.

Stabeno, P.J., Kachel, D.G., Kachel, N.B., Sullivan, M.E., 2005. Observations from moorings in the aleutian passes: temperature, salinity and transport. Fish. Oceanogr. 14 (s1), 39–54.

Suga, T., Aoki, Y., Saito, H., Hanawa, K., 2008. Ventilation of the north pacific subtropical pycnocline and mode water formation. Prog. Oceanogr. 77 (4), 285–297.

Talley, L.D., Nagata, Y., Fujimura, M., Iwao, T., Kono, T., Inagake, D., et al., 1995. North Pacific Intermediate Water in the Kuroshio/Oyashio mixed water region. J. Phys. Oceanogr. 25 (4), 475–501. https://doi.org/10.1175/1520-0485(1995)025<0475:NPIWIT>2.0.CO;2.

Williams, R.G., Roussenov, V., Follows, M.J., 2006. Nutrient streams and their induction into the mixed layer. Global Biogeochem. Cycles 20 (1), n/a–n/a. https://doi.org/10.1029/2005GB002586.

Williams, R.G., McDonagh, E., Roussenov, V.M., Torres-Valdes, S., King, B., Sanders, R., Hansell, D.A., 2011. Nutrient streams in the North Atlantic: Advective pathways of inorganic and dissolved organic nutrients. Global Biogeochem. Cycles 25 (4), GB4008. https://doi.org/10.1029/2010GB003853.

Wunsch, C., 1978. The North Atlantic general circulation west of 50°W determined by inverse methods. Rev. Geophys. 16 (4), 583–620. https://doi.org/10.1029/RG016i004p00583.